Determination of a sodium-ion cell entropy-variation

Nicolas Damay, Rémi Recoquillé, Houssam Rabab, Joanna Kozma, Christophe Forgez, Asmae El Mejdoubi, Khadija El Kadri Benkara

Determination of a sodium-ion cell entropy-variation

Nicolas Damay[a,*], Rémi Recoquillé[a], Houssam Rabab[a,b], Joanna Kozma[a], Christophe Forgez[a], Asmae El Mejdoubi[b], Khadija El Kadri Benkara[a]

[a] *Université de Technologie de Compiègne, Roberval (Mechanics, energy and electricity) Centre de recherche Royallieu, CS 60319, 60203 Compiègne Cedex, France*
[b] *TIAMAT, Hub de l'énergie, 15 rue Baudelocque 80000 Amiens, France*

Abstract

The entropy-variation of a battery is responsible for heat generation or consumption during operation. It is an important part of a thermal model, but it can also provide information on the cell behavior. This study is focused on the determination of the entropy-variation curve of a sodium-ion cell whose cathode is based on $Na_3V_2(PO_4)_2F_3$ and anode on hard carbon (NVPF/HC). The measurement method is a calorimetric approach based on the inversion of a one-node thermal model. It requires a few tests in a climatic chamber, making it accessible for a lot of laboratories. Results obtained at three different current-rates (0.5 C, 1 C and 2 C) are consistent, leading to an entropy-variation curve that varies a lot and is negative over most of the state of charge range (minimum value around -0.5 mV/K). As showed in this article, the associated entropic heat is strongly negative during charge and positive during discharge. This study brings an accurate entropy-variation curve for NVPF/HC cells that can be used for thermal models or for other physical analysis. It also shows that entropy-variation plays an important role in the thermal behavior of NVPF/HC cells and that it should be taken into account when modeling them.

Keywords: Sodium-ion, Batteries, Entropy variation, Calorimetric analysis, Heat generation

1. Introduction

Sodium-ion batteries are considered to have good power density, allowing for high current-rates in charge and discharge, as well as good lifetime [1]. For high-power applications, predicting the thermal behavior is important to help ensure that the battery remains within a safe operating range, either for safety reasons or to limit degradation due to excessive temperatures [2, 3].

Predicting thermal behavior can be done experimentally, but studying all possible use cases requires extensive testing, which is expensive in terms of time and resources. The use of thermal models can often reduce this experimental cost because they require fewer tests to calibrate and can then simulate all cases within the effective range of the model [4, 5, 6, 7].

One tricky part of thermal modeling is the simulation of the heat sources [8]. Generally, they are considered to be due to two main components: the electrical losses and the entropy variation [9]. Electrical losses are highly non-linear regarding the temperature, the current and the state of charge (SoC) [10, 11]. Fortunately, they may be estimated by measuring the current and the voltage of the battery [7]. Regarding the entropic heat, it is generally considered as a function of the SoC only. Schmidt *et al.* [12] proposed an accurate method for measuring the entropy-variation and they demonstrated that it may differ between charge and discharge. This hysteretic behavior can be interesting for the study of the electrochemical reactions occurring in charge and discharge [13, 14], but these differences are often neglected for the purpose of thermal simulations [15, 16].

The determination of the entropy-variation, necessary for simulating the entropic heat, can be done by the potentiometric method, in which the variation of the open circuit voltage (OCV) with respect to the temperature is measured for several SoC to create a lookup table [17, 18, 19, 20]. This method requires a lot of tests to obtain a table with a sufficient resolution. On the contrary, calorimetric methods bring results with a high-resolution, but the study of the heat generation has to be done in very specific conditions to accurately extract the entropic heat and compute the entropy-variation [12, 21].

Because commercial sodium-ion cells are more recent than lithium-ion ones, there are very few studies about the entropy-variation of sodium-ion batteries. Huang *et al.* [22] have determined the entropic change of NVPF/HC based sodium-ion cells by a calorimetric approach, but the measurement method is difficult to implement because it uses optical fibers placed inside the studied cells to get their internal temperature. They then extracted the entropic heat by subtracting the electrical losses from the total heat generated, but it requires an accurate estimate of the OCV of the cell, which is highly nonlinear with re-

*Corresponding author
Email address: nicolas.damay@utc.fr (Nicolas Damay)

spect to the SoC.

Wei *et al.* [23] measured the entropy-variation of half cells and full cells made of $Na_3V_2(PO_4)_3$ (NVP) and hard carbon. However, the NVP material for the cell cathode is different from the NVPF of the cells studied in this article. Also, the hard carbon they studied has an OCV with a very typical shape that cannot be distinguished within the OCV of the cells studied here (see section 4.3). This can be due to different levels of disorder in these carbon-based anodes and can lead to substantial differences in their entropy variations, as reported by Reynier *et al.* [24].

In this paper, the entropy change of a sodium-ion battery is determined by a calorimetric approach developed by our team a few years ago [25]. This method was validated for a Li-ion battery, but we will show in this study that it is also applicable to the sodium-ion battery under study. Its main advantage is its simplicity, as it requires only a climate chamber and a temperature measurement of the cell surface. The studied battery is a commercial 18650 cylindrical cell that has been manufactured by the startup Tiamat. Its positive electrode is based on $Na_3V_2(PO_4)_2F_3$ (NVPF) and its negative electrode is based on hard carbon (HC). Its nominal capacity is 700 mAh, its mass is 34 g, its voltage range is between 2 V and 4.25 V, its temperature range is -20 °C to 55 °C for discharge and 0 °C to 55 °C for charge. Its maximal current rates in charge and discharge are respectively 14 C and 20 C for a duration of 10 s. In section 2, the analysis for extracting the entropy-variation from the cell total heat generation is explained. In section 3, the heat generation determination method, based on the inversion of a thermal model, is presented. Finally, a NVPF/HC sodium-ion cell is tested and its entropy-variation is determined and discussed in section 4.

2. Extracting entropy-variation from the cell heat generation

2.1. Definitions

The entropy variation ΔS is related to structural changes of the active materials during operation. The corresponding energy variations may result in heat generation or consumption depending on the SoC and if the current sign is either positive or negative. This behavior can be modeled by Equation 1 in which $\dot{Q}_{\Delta S}$ is the so-called "entropic heat", I is the current (defined as positive during charge), T is the absolute temperature (in Kelvin), n is the number of exchanged electrons during the reaction and F is the Faraday constant [8].

$$\dot{Q}_{\Delta S} = I\,T\,\frac{\Delta S(SoC)}{nF} = I\,T\,\frac{\partial U_{oc}}{\partial T}(SoC) \qquad (1)$$

The term $\Delta S/nF$ is equivalent to the variation of the open-circuit voltage U_{oc} regarding temperature $\partial U_{oc}/\partial T$ [8]. For more convenience, the latter will also be called "entropy variation" in this paper. This coefficient is assumed to be constant within the operating temperature range of the studied cell [5, 12, 22].

Thanks to Equation 1, the entropy variation $\partial U_{oc}/\partial T$ can be derived from the entropic heat. However, the entropic heat is mixed with other heat sources during a battery operation, namely: electrical losses, entropic heat, heat generated by side reaction(s) and heat of mixing [5].

Electrical losses $\dot{Q}_{elec}$ are positive during charge and during discharge (irreversible heat), but they can be different because of non-linearities regarding current, temperature and SoC (Equations 2). These losses can be expressed as the current I times the voltage drop ΔV that appears during operation. ΔV may be obtained by measuring the cell voltage U_{cell} and estimating the OCV U_{oc}. In this study, the electrical losses are not measured because the experimental conditions will lead to them having a very low impact for the determination of the entropy-variation $\partial U_{oc}/\partial T$ (see part 2.2).

$$\begin{aligned} \dot{Q}_{elec} &= I \times \Delta V(SoC, I, T) \\ \dot{Q}_{elec} &= I \times (U_{cell} - U_{oc}) \end{aligned} \qquad (2)$$

Concerning the studied battery, side reactions are mostly aging reactions that are slow enough for their heat generation to be neglected. The heat of mixing is negative during the creation of concentration gradients and is positive when these gradients disappear (the sum being zero) [8]. If the concentration gradients are small enough, e.g. for cells with good transport properties and low current operation, the heat of mixing can be neglected. In this study, the cell is only powered at low currents compared to its maximum capacity (from C/2 to 2C). Consequently, only electrical losses $\dot{Q}_{elec}$ and entropic heat $\dot{Q}_{\Delta S}$ are considered in the total heat generation $\dot{Q}_{tot}$ (Equations 3).

$$\begin{aligned} \dot{Q}_{tot} &= \dot{Q}_{elec} + \dot{Q}_{\Delta S} \\ \dot{Q}_{tot} &= I\ \Delta V(SoC, I, T) + I\ T\ \frac{\partial U_{oc}}{\partial T}(SoC) \end{aligned} \qquad (3)$$

In order to compare the total heat generated in charge $\dot{Q}_{tot,Ch}$ and discharge $\dot{Q}_{tot,Dch}$, it is convenient to rewrite Equations (3) with the absolute value of the current $|I|$ to bring Equations (4). They respect the fact that the electrical losses are always positive (irreversible heat) and that the current sign has to be considered for the entropic heat (reversible heat). Both electrical losses and entropic heat depend on the actual temperature during charging (noted T_{Ch}) and discharging (noted T_{Dch}).

$$\dot{Q}_{tot,Ch} = |I| \left[|\Delta V_{Ch}(SoC, I, T_{Ch})| + T_{Ch} \frac{\partial U_{oc}}{\partial T}(SoC) \right]$$
$$\dot{Q}_{tot,Dch} = |I| \left[|\Delta V_{Dch}(SoC, I, T_{Dch})| - T_{Dch} \frac{\partial U_{oc}}{\partial T}(SoC) \right] \quad (4)$$

2.2. Determination of the entropy variation

The entropy variation can be isolated by subtracting $\dot{Q}_{tot,Dch}$ from $\dot{Q}_{tot,Ch}$, leading to Equation 5. In this purpose, they need to be run with the same current rate. Please note that every term is expressed as a function of the SoC.

$$\frac{\partial U_{oc}}{\partial T}(SoC) = \frac{\dot{Q}_{tot,Ch} - \dot{Q}_{tot,Dch} - \Delta\dot{Q}_{Elec}}{|I| \ (T_{Ch} + T_{Dch})} \quad (5)$$

$\Delta\dot{Q}_{Elec}$ is the difference between the electrical losses during charge and discharge and is expressed by Equation 6.

$$\begin{aligned} \Delta\dot{Q}_{Elec} &= \dot{Q}_{elec,Ch} - \dot{Q}_{elec,Dch} \\ \Delta\dot{Q}_{Elec} &= |I| \left(|\Delta V_{Ch}| - |\Delta V_{Dch}| \right) \end{aligned} \quad (6)$$

$\Delta\dot{Q}_{Elec}$ is not trivial to estimate and thus brings a source of uncertainty to $\partial U_{oc}/\partial T$ estimation [7]. The precision of this method relies on making $\Delta\dot{Q}_{Elec}$ as negligible as possible compared to the entropic heat by using an experimental protocol that maximize the relative contribution of entropic heat compared to electrical losses.

The first way to reduce $\Delta\dot{Q}_{Elec}$ is to increase the operating temperature of the cell T. Thus, the cell impedance and its electrical losses decreases [26], making the entropic heat more significant in the total heat generation. Besides, the entropic heat slightly increases in these conditions (see Equation 1).

The second way to reduce $\Delta\dot{Q}_{Elec}$ is to decrease the current I. As a matter of fact, the entropic heat is proportional to the current and electrical losses are approximately proportional to the squared current. Consequently, at low current operation, the entropic heat will be relatively high compared to electrical losses [25]. Nevertheless, the cell must generate a minimum of heat to ensure its accurate estimation. Three current rates have been tested, analyzed, and their results will be compared in section 4.

In these conditions, $\Delta\dot{Q}_{Elec}$ is assumed to be negligible (this will be verified in section 4.3). In these operating conditions, the entropy variation would hence be approximated by Equation 7 and by:

- estimating the heat generations $\dot{Q}_{tot,Ch}$ and $\dot{Q}_{tot,Dch}$;
- measuring the temperature T_{Ch} and T_{Dch}.

$$\frac{\partial U_{oc}}{\partial T}(SoC) \approx \frac{\dot{Q}_{tot,Ch}(SoC) - \dot{Q}_{tot,Dch}(SoC)}{|I| \ (T_{Ch}(SoC) + T_{Dch}(SoC))} \quad (7)$$

The generated heats $\dot{Q}_{tot,Ch}$ and $\dot{Q}_{tot,Dch}$ are estimated thanks to the inversion of a one node thermal model. The latter and its parameters determinations are presented in the next section.

3. Cell heat generation estimation

3.1. Thermal model presentation

A thermal model is often used for predicting a temperature evolution, but it can also be inverted to estimate the generated heat [5, 22]. It thereby requires the knowledge of its parameters, the external conditions and the temperature evolution.

During the entropy variation test, the cell is thermally insulated, so it can be assumed to be homogeneous during operation. Hence, its temperature can be measured on its surface and a one-node thermal model can be used (Figure 1). The latter has two parameters: one heat capacity C_{th} and one thermal resistance R_{th} toward the cell environment. The total heat generation $\dot{Q}_{tot}$ and the external temperature T_{ext} (that is ambient air temperature) are equivalent to a current and a voltage sources respectively.

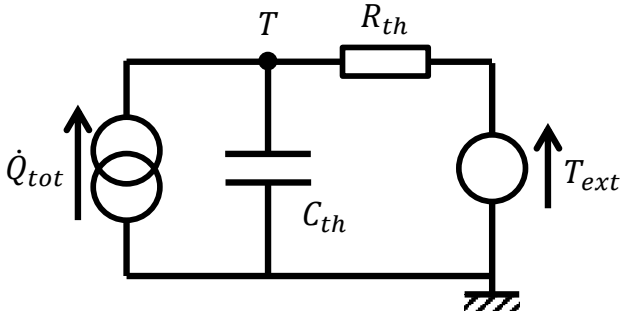

Figure 1: Thermal model of an isothermal cell

The state equation corresponding to this model can be obtained thanks to Kirchhoff's laws (Equation 8) where T is the temperature of the cell. Before using it to estimate $\dot{Q}_{tot,Ch}$ and $\dot{Q}_{tot,Dch}$, the heat capacity C_{th} and the equivalent thermal resistance R_{th} values have to be measured.

$$\dot{Q} = C_{th} \frac{dT}{dt} + \frac{T - T_{ext}}{R_{th}} \quad (8)$$

The thermal resistance R_{th} is measured during the rest phases of the test used for the entropy variation estimation. Its determination will be presented in the section 4.

3.2. Heat capacity determination

As for the heat capacity C_{th}, it has been measured using the setup shown on Figure 2. The cell was connected to a Bio-Logic system that can generate and measure current

or voltage with a precision of 0.1% of its full scale (that is ± 20 A with ± 10 V). It was packed with polyurethane foam to ensure that the internal thermal resistance (from the cell core to its surface) is negligible compared to the external thermal resistance (from the cell surface to the ambient air). This is important to respect the assumptions of an isothermal cell, made in section 3.1.

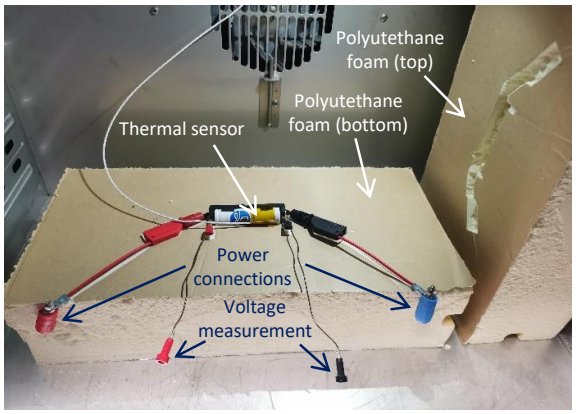

Figure 2: Experimental setup for heat capacity and entropy-variation determination. The cell is covered with polyurethane foam and put within a climate chamber.

A ± 4 A (± 5.7 C) square current with a period T of 2 s has been applied to the cell in order to create a heat generation step. The 2-second-long period has been chosen because it is very small compared to the thermal time constant of the cell and it allowed a sufficient heat generation rate. The thermal time constant is the product of C_{th} and R_{th} and its value is about 1 h for the experimental setup of Figure 2. Thus, the average heat generation $\dot{Q}_{avg}$ can be used in this calculus instead of the instantaneous heat generation. Besides, the $\dot{Q}_{avg}$ measurement is simple and accurate in these conditions. The SoC and the OCV remain constant and, as the mean current is equal to zero, the mean reversible heat is also equal to zero. Thus, only electrical losses contribute to the cell heating. They can be measured according to Equation 9 by:

- measuring the OCV (U_{oc}) before beginning the test (the cell being at equilibrium);
- measuring the current I_{cell} and the cell voltage U_{cell} during the test [7].

$$\begin{aligned} \dot{Q}_{avg}(t) &= \frac{1}{T}\int_{t-T/2}^{t+T/2} \dot{Q}_{elec}.dt \\ \dot{Q}_{avg}(t) &= \frac{1}{T}\int_{t-T/2}^{t+T/2} I_{cell}\ (U_{cell} - U_{oc}).dt \end{aligned} \tag{9}$$

At the very beginning of the test, the last term in Equation 8 can be neglected, because the difference between T and T_{ext} is very small (quasi-adiabatic conditions). Moreover, the cell is assumed to be subjected to a heat generation step. Consequently, its temperature T increases as a ramp (Figure 3) and the heat capacity can be determined by Equation 10. It has been found to be equal to 50.1 $J.K^{-1}$ (calculus made between 2 min and 5 min). As the mass M of the cell is 34 g, this brings an averaged specific heat C_p of 1.47 $J.K^{-1}.g^{-1}$ (Equation 11). Based on literature, specific heat values vary according to the battery technology used. For example with lithium-ion batteries, we found a range value of 1.1 to 1.72 $J.K^{-1}.g^{-1}$ for $LiFePO_4$ (LFP) and a range value of 0.84 to 1.18 $J.K^{-1}.g^{-1}$ for $LiNiMnCoO_2$ (NMC) [27, 28, 29, 30].

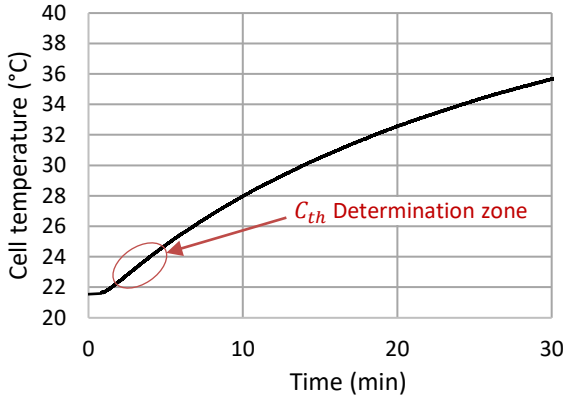

Figure 3: Test for heat capacity determination. Thermal response to a ± 4 A (5.7 C) square current with a period T of 2 s.

$$C_{th} = \frac{\dot{Q}_{avg}}{dT/dt} = 50.1\ J.K^{-1} \tag{10}$$

$$C_p = \frac{C_{th}}{M} = 1.47\ J.K^{-1}.g^{-1} \tag{11}$$

4. Application to a NVPF/HC sodium-ion cell

4.1. Experimental protocol for entropy variation determination

The cell has been insulated as for the heat capacity determination. The aim of this experimental setup is to minimize the cell cooling, so it can be assumed to be isothermal. It has been put in a climatic chamber at 40 °C and:

- fully charged by the constant current constant voltage (CCCV) method;
- left at rest until it reached the thermal equilibrium;
- fully discharged and left to rest for several hours;
- fully charged with the same current and left to rest for several hours.

Between each step, the cell has been left at rest until its temperature reaches the chamber temperature (±1 °C).

This keeps it from overheating and it allows the determination of R_{th}.

This test has been carried out three times, with three different current values for the charging and discharging steps: 350 mA (0.5 C), 700 mA (1 C) and 1.4 A (2 C). This will bring three different estimations of the entropy variation $\partial U_{oc}/\partial T$, which will be compared and discussed in the next section.

4.2. Thermal resistance and heat generation determinations

The temperature evolution of the cell and the corresponding heat generation have been reported on Figure 4a for the 1 C test. Whereas the climatic chamber temperature had been set to 40 °C, the cell temperature stabilized around 41 °C at the end of the test, certainly because the climatic chamber thermal sensor has a small bias. Consequently, the cell temperature at the beginning of the test was not exactly at equilibrium, but this doesn't affect the analysis, nor the conclusions of this study. The evolution of the state of charge during the test has been reported on Figure 4b for a better understanding.

In order to keep the thermal model and its parameter determination as simple as possible, the external temperature T_{ext} in Equation 8 is replaced by the equilibrium temperature T_{eq}, corresponding to the steady-state with no heat generation, to bring Equation 12.

$$\dot{Q} = C_{th}\frac{dT}{dt} + \frac{T - T_{eq}}{R_{th}} \tag{12}$$

To ensure the best heat generation estimation, the equilibrium temperature T_{eq} and the equivalent thermal resistance R_{th} have been determined using an optimization algorithm during the first rest period (between 1 h and 3.5 h). In these conditions, the total heat generation is assumed to be equal to zero. Consequently, Equation 12 can be simplified to bring Equation 13. We used the *lsqcurvefit* function of the MATLAB software to fit this equation to the chosen data. The optimal values for R_{th} and T_{eq} have been found to be respectively equal to 61.9 $K.W^{-1}$ and 41.0 °C.

$$C_{th}\frac{dT}{dt} + \frac{T - T_{eq}}{R_{th}} = 0 \tag{13}$$

All the parameters of the thermal model being determined, the heat generation reproduced on Figure 4a can be estimated using Equation 12. The cell temperature T was measured and the derivative dT/dt was estimated by a linear regression, carried on a time interval centered on the calculation points. For the 1 C test of Figure 4a, we found that intervals of 150 s during the discharge and charge and 400 s during rest periods were good compromises between the noise reduction and the heat generation estimation accuracy.

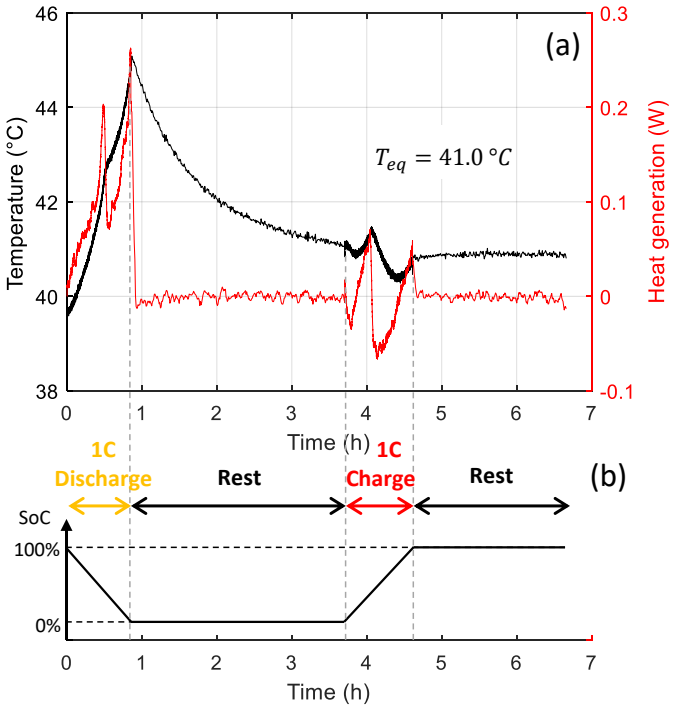

Figure 4: (a) Thermal response and measured heat generation for 1C discharge and charge. The equilibrium temperature T_{eq} is 41.0 °C. (b) Corresponding state of charge.

a

4.3. Results and discussions

Similar evolutions can be observed during the charge and the discharge on Figure 4a. Both heat generation curves grow continuously with an important drop around the middle of the cycle. However, the mean amplitude of the heat-generation is far more important during discharge than during the charge, whose average is close the zero. It can be noticed that the temperature even goes below the equilibrium temperature of the cell between 4 and 5 h because of a negative total heat generation $\dot{Q}_{tot}$. These variations have been found for every current rate considered and we found that they are mostly caused by the entropic heat, as discussed below.

Figure 5a has been made to underline the heat source separation. The total heat generation in charge and discharge, respectively $\dot{Q}_{tot,Ch}$ and $\dot{Q}_{tot,Dch}$, are plotted as functions of the SoC. From Equations 4, we derived estimates for electrical losses $\dot{Q}_{elec}$ and entropic heat $\dot{Q}_{\Delta S}$ (Equations 14) and reported them on Figure 5a. These equations are based on the irreversible and reversible behaviors of $\dot{Q}_{elec}$ and $\dot{Q}_{\Delta S}$. Please note that the estimated heat generations are slightly biased near 0% SoC and 100% SoC, because of the T derivative calculus smooths quick variations.

$$\dot{Q}_{elec} \approx \frac{\dot{Q}_{tot,Ch} + \dot{Q}_{tot,Dch}}{2}$$
$$\dot{Q}_{\Delta S} \approx \frac{\dot{Q}_{tot,Ch} - \dot{Q}_{tot,Dch}}{2} \quad (14)$$

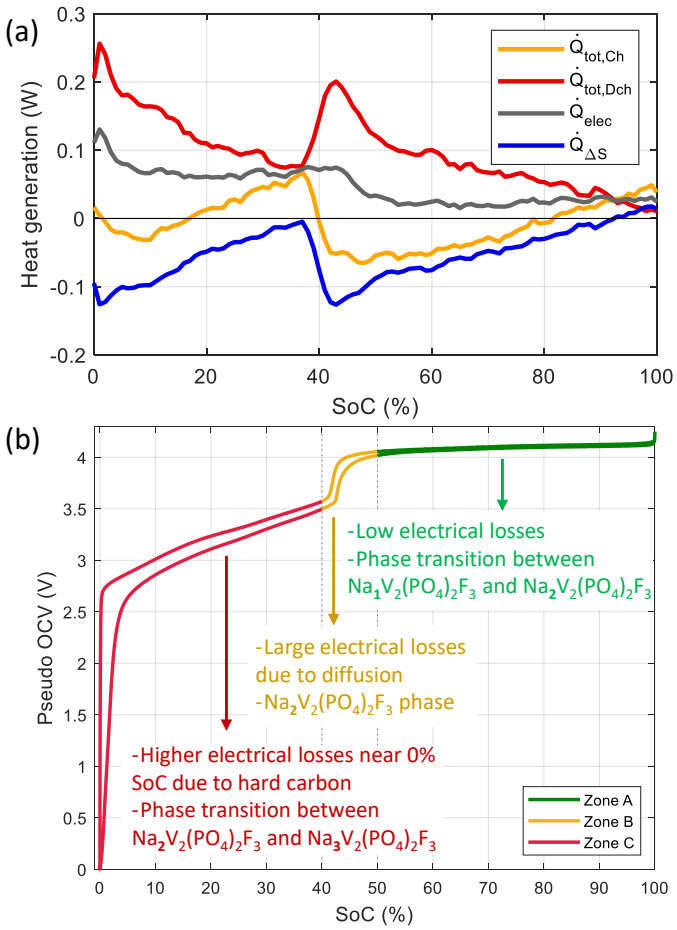

Figure 5: (a) Heat generation in charge and discharge, entropic heat and electrical losses (1 C test). (b) Corresponding pseudo-OCV in charge and discharge, close to U_{oc}, measured at C/50.

In order to go deeper into the analysis of the results, the pseudo-OCV (noted OCV for the sake of simplicity) of the studied cell, measured at C/50 has also been reported on Figure 5b. The entropic heat evolution is naturally consistent with the OCV. Two distinct phase transitions occur during a complete charge or discharge, namely:

- in zone A of the OCV (for SoC between 50% and 100%), a transition between $Na_1V_2(PO_4)_2F_3$ and $Na_2V_2(PO_4)_2F_3$;
- in zone C of the OCV (for SoC between 0% and 40%), another transition between $Na_2V_2(PO_4)_2F_3$ and $Na_3V_2(PO_4)_2F_3$ [31].

These phase transitions corresponds to two different states that have different entropy variation values, which explains the important change of entropic heat in the middle of the cycles. Around 40% - 50% (zone B of the OCV), the positive electrode is close to a pure $Na_2V_2(PO_4)_2F_3$ phase [31]. The hard-carbon-based negative electrode also contribute to the entropy-variation and might be responsible for the $\dot{Q}_{\Delta S}$ slope, but the contributions of both electrodes cannot be separated with the method used in this article.

Regarding the electrical losses, they are also in correspondence with the OCV, as they are low for higher SoC (Zone A on Figure 5b). In zone B, $\dot{Q}_{elec}$ increases because of a large OCV variation (about 0.5 V), leading to strong diffusion effects, hence generating more heat. In zone C, there is an increase of the electrical losses near 0% SoC, maybe due to the adsorption of sodium ions on the hard carbon in this operating range [32, 33, 34].

The entropy variation – corresponding to the entropic heat of Figure 5a – has been reported on Figure 6, along with the results obtained *via* C/2 and 2C tests. The three current rates lead to close entropy-variation curves and their mean is also represented on Figure 6. This confirms that neglecting $\Delta\dot{Q}_{Elec}$ is reasonable, as assumed in section section 2. In this view, results obtained through C/2 charge and discharge are bound to be the most precise because the electrical losses are at their lowest compared to entropic heat.

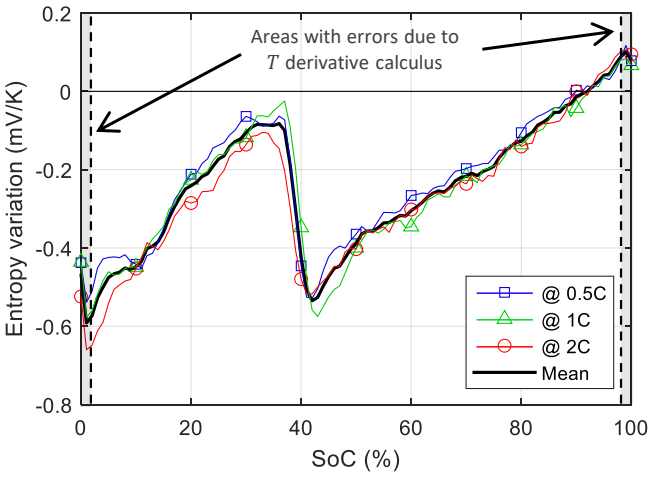

Figure 6: Entropy variation $\partial U_{oc}/\partial T$ of a NVPF/HC sodium-ion cell obtained with the calorimetric method at different current rates and their mean value. Root mean squared errors between the mean value and results at 0.5 C, 1 C and 2 C are respectively: 0.027 mV/K, 0.026 mV/K and 0.034 mV/K.

The entropy variation $\partial U_{oc}/\partial T$ of sodium-ion battery is essentially negative meaning that the entropic heat is mostly positive during discharges and strongly negative during charges. As a result, more heat is generated during the discharge. However, a use of these batteries in electric vehicles would result in discharges at low current-rates in average, thus giving more time to the cooling system to evacuate the heat. Also, a use in hybrid vehicle – in which the mean SoC of the battery does not change much

– will tend to strongly reduce the entropic heat. There is a strong interest for fast charge applications as the higher heat generation from electrical sources would be partially compensated by the negative entropic heat, thus helping to charge the battery quickly even if it has already been heated up by a previous use.

5. Conclusion

The entropy-variation of a sodium-ion battery (NVPF/HC) was determined using a calorimetric method. The heat generated during charges and discharges at constant current has been determined by inverting a thermal model. The two contributions to the total heat generation, namely entropic heat (reversible heat) and electrical losses (irreversible heat), were later separated and identified in order to obtain the entropy-variation $\partial U_{oc}/\partial T$ as a function of SoC.

The entropy-variation results are obtained with three different current rates and are close to each other, thus demonstrating their consistency. Moreover, we showed that the evolution of the entropy-variation $\partial U_{oc}/\partial T$ is closely related to the cell OCV and to the phase transitions in the positive electrode (NVPF).

The studied batteries have a strongly negative entropy-variation, thus leading to a positive heat generation during discharge. This has to be considered for designing the cooling system of such batteries if they are used for fast discharge. However, the entropic heat would be strongly negative during charge, thus mitigating the effects of electrical losses for fast charging applications.

Acknowledgement

The authors would like to thank the startup Tiamat for providing the sodium-ion batteries studied here.

References

[1] J. M. Tarascon, Na-ion versus Li-ion Batteries: Complementarity Rather than Competitiveness, Joule 4 (8) (2020) 1616–1620. doi:10.1016/j.joule.2020.06.003.

[2] A. Cordoba-Arenas, S. Onori, G. Rizzoni, A control-oriented lithium-ion battery pack model for plug-in hybrid electric vehicle cycle-life studies and system design with consideration of health management, Journal of Power Sources 279 (2015) 791–808. doi:10.1016/j.jpowsour.2014.12.048.

[3] T. R. Tanim, C. D. Rahn, Aging formula for lithium ion batteries with solid electrolyte interphase layer growth, Journal of Power Sources 294 (2015) 239–247. doi:10.1016/j.jpowsour.2015.06.014.

[4] S. Al Hallaj, H. Maleki, J.-S. Hong, J. R. Selman, Thermal modeling and design considerations of lithium-ion batteries, Journal of Power Sources 83 (1999) 1–8. doi:10.1016/S0378-7753(99)00178-0.

[5] C. Forgez, D. Vinh Do, G. Friedrich, M. Morcrette, C. Delacourt, Thermal modeling of a cylindrical $LiFePO_4$/graphite lithium-ion battery, Journal of Power Sources 195 (9) (2010) 2961–2968. doi:10.1016/j.jpowsour.2009.10.105.

[6] X. Lin, H. E. Perez, S. Mohan, J. B. Siegel, A. G. Stefanopoulou, Y. Ding, M. P. Castanier, A lumped-parameter electro-thermal model for cylindrical batteries, Journal of Power Sources 257 (2014) 1–11. doi:10.1016/j.jpowsour.2014.01.097.

[7] N. Damay, C. Forgez, M.-P. Bichat, G. Friedrich, Thermal modeling of large prismatic $LiFePO_4$/graphite battery . Coupled thermal and heat generation models for characterization and simulation, Journal of Power Sources 283 (2015) 37–45. doi:10.1016/j.jpowsour.2015.02.091.

[8] K. E. Thomas, J. Newman, Heats of mixing and of entropy in porous insertion electrodes, Journal of Power Sources 119-121 (2003) 844–849. doi:10.1016/S0378-7753(03)00283-0.

[9] T. M. Bandhauer, S. Garimella, T. F. Fuller, A Critical Review of Thermal Issues in Lithium-Ion Batteries, Journal of The Electrochemical Society 158 (3) (2011) R1. doi:10.1149/1.3515880.

[10] L. Gagneur, A. Driemeyer-Franco, C. Forgez, G. Friedrich, Modeling of the diffusion phenomenon in a lithium-ion cell using frequency or time domain identification, Microelectronics Reliability 53 (6) (2013) 784–796. doi:10.1016/j.microrel.2013.03.009.

[11] J. Illig, Physically based Impedance Modelling of Lithium-ion Cells, Ph.D. thesis (2014).

[12] J. P. Schmidt, A. Weber, E. Ivers-Tiffée, A novel and precise measuring method for the entropy of lithium-ion cells: ΔS via electrothermal impedance spectroscopy, Electrochimica Acta 137 (2014) 311–319. doi:10.1016/j.electacta.2014.05.153.

[13] R. Yazami, Y. Reynier, Thermodynamics and crystal structure anomalies in lithium-intercalated graphite, Journal of Power Sources 153 (2) (2006) 312–318. doi:10.1016/j.jpowsour.2005.05.087.

[14] D. Ahn, R. Raj, Thermodynamic measurements pertaining to the hysteretic intercalation of lithium in polymer-derived silicon oxycarbide, Journal of Power Sources 195 (12) (2010) 3900–3906. doi:10.1016/j.jpowsour.2009.12.116.

[15] A. Eddahech, O. Briat, J.-M. Vinassa, Thermal characterization of a high-power lithium-ion battery: Potentiometric and calorimetric measurement of entropy changes, Energy 61 (2013) 432–439. doi:10.1016/j.energy.2013.09.028.

[16] M. Shadman Rad, D. L. Danilov, M. Baghalha, M. Kazemeini, P. H. Notten, Adaptive thermal modeling of Li-ion batteries, Electrochimica Acta 102 (2013) 183–195. doi:10.1016/j.electacta.2013.03.167.

[17] R. E. Williford, V. V. Viswanathan, J.-G. Zhang, Effects of entropy changes in anodes and cathodes on the thermal behavior of lithium ion batteries, Journal of Power Sources 189 (1) (2009) 101–107. doi:10.1016/j.jpowsour.2008.10.078.

[18] V. V. Viswanathan, D. Choi, D. Wang, W. Xu, S. Towne, R. E. Williford, J.-G. Zhang, J. Liu, Z. Yang, Effect of entropy change of lithium intercalation in cathodes and anodes on Li-ion battery thermal management, Journal of Power Sources 195 (11) (2010) 3720–3729. doi:10.1016/j.jpowsour.2009.11.103.

[19] K. Jalkanen, K. Vuorilehto, Entropy change characteristics of $LiMn_{0.67}Fe_{0.33}PO_4$ and $Li_4Ti_5O_{12}$ electrode materials, Journal of Power Sources 273 (2015) 351–359. doi:10.1016/j.jpowsour.2014.09.091.

[20] I. Zilberman, A. Rheinfeld, A. Jossen, Uncertainties in entropy due to temperature path dependent voltage hysteresis in Li-ion cells, Journal of Power Sources 395 (May) (2018) 179–184. doi:10.1016/j.jpowsour.2018.05.052.

[21] A. M. Ahmad, G. Thenaisie, S. G. Lee, A calorimetric approach to fast entropy-variations extraction for lithium-ion batteries using optimized galvanostatic intermittent titration technique, Journal of Power Sources Advances 16 (June) (2022) 100097. doi:10.1016/j.powera.2022.100097.

[22] J. Huang, L. Albero Blanquer, J. Bonefacino, E. R. Logan, D. Alves Dalla Corte, C. Delacourt, B. M. Gallant, S. T. Boles, J. R. Dahn, H. Y. Tam, J. M. Tarascon, Operando decoding of chemical and thermal events in commercial Na(Li)-ion cells via optical sensors, Nature Energy 5 (9) (2020) 674–683. doi:10.1038/s41560-020-0665-y.

[23] F. Wei, P. Li, Q. Zhang, G. Shao, J. Mao, Entropy Change

Characteristics for Sodium Ion Half/Full Cells Based on $Na_3V_2(PO_4)_3$ and Hard Carbon Materials, Journal of The Electrochemical Society 169 (5) (2022) 050503. doi:10.1149/1945-7111/ac6a14.

[24] Y. F. Reynier, R. Yazami, B. Fultz, Thermodynamics of Lithium Intercalation into Graphites and Disordered Carbons, Journal of The Electrochemical Society 151 (3) (2004) A422–A426. doi:10.1149/1.1646152.

[25] N. Damay, C. Forgez, M.-P. Bichat, G. Friedrich, A method for the fast estimation of a battery entropy-variation high-resolution curve – Application on a commercial $LiFePO_4$/graphite cell, Journal of Power Sources 332 (2016) 149–153. doi:10.1016/j.jpowsour.2016.09.083.

[26] N. Damay, K. Mergo Mbeya, G. Friedrich, C. Forgez, Separation of the charge transfers and solid electrolyte interphase contributions to a battery voltage by modeling their non-linearities regarding current and temperature, Journal of Power Sources 516 (2021) 230617. doi:10.1016/j.jpowsour.2021.230617.

[27] P. Jindal, R. Katiyar, J. Bhattacharya, Evaluation of accuracy for Bernardi equation in estimating heat generation rate for continuous and pulse-discharge protocols in LFP and NMC based Li-ion batteries, Applied Thermal Engineering 201 (2022) 117794. doi:10.1016/j.applthermaleng.2021.117794.

[28] T. S. Bryden, B. Dimitrov, G. Hilton, C. Ponce de León, P. Bugryniec, S. Brown, D. Cumming, A. Cruden, Methodology to determine the heat capacity of lithium-ion cells, Journal of Power Sources 395 (2018) 369–378. doi:10.1016/j.jpowsour.2018.05.084.

[29] S. Drake, D. Wetz, J. Ostanek, S. Miller, J. Heinzel, A. Jain, Measurement of anisotropic thermophysical properties of cylindrical Li-ion cells, Journal of Power Sources 252 (2014) 298–304. doi:10.1016/j.jpowsour.2013.11.107.

[30] N. Nieto, L. Díaz, J. Gastelurrutia, I. Alava, F. Blanco, J. Carlos Ramos, A. Rivas, Thermal Modeling of Large Format Lithium-Ion Cells, Journal of The Electrochemical Society 160 (2) (2013) A212–A217. doi:10.1149/2.042302jes.

[31] S. Yuvaraj, W. Oh, W. S. Yoon, Recent progress on sodium vanadium fluorophosphates for high voltage sodium-ion battery application, Journal of Electrochemical Science and Technology 10 (1) (2019) 1–13. doi:10.5229/JECST.2019.10.1.1.

[32] H. Rabab, N. Damay, F. Vendrame, C. Forgez, A. El Mejdoubi, Modeling the non-linearities of charge-transfers and solid electrolyte interphase resistances for a sodium-ion battery with a hard carbon electrode, in: ELECTRIMACS 2022, Nancy, 2022.

[33] C. Matei Ghimbeu, J. Górka, V. Simone, L. Simonin, S. Martinet, C. Vix-Guterl, Insights on the Na^+ ion storage mechanism in hard carbon: Discrimination between the porosity, surface functional groups and defects, Nano Energy 44 (December 2017) (2018) 327–335. doi:10.1016/j.nanoen.2017.12.013.

[34] L. F. Zhao, Z. Hu, W. H. Lai, Y. Tao, J. Peng, Z. C. Miao, Y. X. Wang, S. L. Chou, H. K. Liu, S. X. Dou, Hard Carbon Anodes: Fundamental Understanding and Commercial Perspectives for Na-Ion Batteries beyond Li-Ion and K-Ion Counterparts, Advanced Energy Materials 11 (1) (2021) 1–28. doi:10.1002/aenm.202002704.